Article

Research on Fault Activation and Its Influencing Factors on the Barrier Effect of Rock Mass Movement Induced by Mining

Yanhui Guo [1,*], Luo Luo [1] and Chuangye Wang [2]

1 Faculty of Public Safety and Emergency Management, Kunming University of Science and Technology, Kunming 650093, China
2 Engineering Technology Research Institute of PetroChina Coalbed Methane Co., Ltd., Xi'an 710082, China
* Correspondence: guoyanhui0818@kust.edu.cn

Abstract: For the study of the driving forces behind fault activation and its influencing factors on the barrier effect of rock mass movement under the influence of mining, the discrete element numerical simulation software 3DEC was used for the analysis of the impact on the distance to mining area from fault, the buried depth of the upper boundary of the fault, the dip angle of fault, the size of the mining area and the thickness of the fault zone respectively. The results show that the mining areas are closer to the fault as distances decrease, the burial depth of the upper boundary of the fault increases, and the size of the mining area increases, the fault is easier to activate, and fault activation has a stronger barrier impact on displacement field and stress field propagation. When the fault is cut into the goaf, the difference of rock displacement in both directions of the fault increases when the dip of the fault increases, and the fault is more susceptible to instability and activation. The barrier strength grows with the increase of the thickness of the fault fracture zone. The results of this study have important implications for the guard against and control of deep mining-related fault activation disasters.

Keywords: fault activation; mining impact; rock mass movement; barrier effect; 3DEC

1. Introduction

With the acceleration of urbanization and industrialization, the demand of human society for mineral resources continues to increase [1]. With the increasing scale of underground mining, mine disasters are becoming more and more serious [2,3]. A fault is an inevitable major geological structure in the mining of underground mines, which will alter the stress and displacement fields of the surrounding rock, destroying the continuity and stability of the rock layers [4,5]. During deep underground mine extraction, various influencing factors will lead to fault activation, resulting in mining disasters. For example, rock bursting, mine water gushing, and mining area collapse on the surface [6–9]. Thus, one of the key elements impacting underground safe mining has been fault activation [10–12]. At the same time, during large-scale underground mine extraction, the faults distributed within the mining influence range will become a barrier for rock mass movement, deformation, and mining stress propagation [13]. In addition, due to the unclear understanding of the barrier effect of faults on rock mass movement, the unreasonable design of underground mine shaft and roadway engineering will lead to the abandonment of shaft and roadway engineering. This could have a great influence on the green, efficient as well as safe exploitation of mines [14,15]. The key factors affecting the barrier effect of fault activation rock mass movement include the distance between the mining area and the fault, the burial depth of the upper boundary of the fault, the fault dip angle, the size of the mining area, and the thickness of the fault zone. Therefore, the analysis of influencing factors on the barrier effect of rock mass movement under the influence of mining is of great significance in preventing and controlling the related disasters caused by the fault activation in deep mining of underground mines.

Numerous academics have studied that the influencing factors of fault activation and its barrier effect caused by mining in recent years. In terms of fault activation law and mechanism analysis, Jiang et al. [16] studied and analyzed the stress and rock mass movement characteristics in the process of fault activation of coal seams through three-dimensional numerical calculations. Nguyen and Rutqvist et al. [17–19] developed a mathematical model to simulate the fault activation during the controlled water injection experiment of the fault in the "Mont Terri Underground Research Laboratory" in Switzerland. Based on this, they also carried out a series of controlled fault activation experiments in clay. Jiang et al. [20] studied the space-time evolution law of the normal and shear stresses at the contact surface of the fault as well as the law of movement in the fault hanging wall and footwall through simulation. Zhao [21] studied the ground pressure behavior and dynamic response characteristics before and after fault activation under the influence of mining by establishing a similar model based on the actual project. Some scholars have studied fault activation through indoor experiments, Ohno et al. [22] conducted injection tests and repeated packer tests on siliceous mudstone faults, which can effectively evaluate the sensitivity of fault hydraulic fracturing to fault activation. Chen and Gong et al. [23–25] used acoustic emission technology to unite RFPA software to simulate and analyze the failure process of deep rock joints, and revealed the failure mechanism of deep jointed rock mass during excavation. Mngadi and Nguyen et al. [26,27] carried out friction experiments of different groups on rocks from deep mining in high-stress areas, and described the propagation process of the fracture along the underground brittle shear zone, which is of great significance to the study of rockburst. Li et al. [28] studied the stress environment and conditions of various fault activation and think that mining would cause uneven changes in vertical stress and horizontal stress in the fault, which was easy to induce fault activation.

The formation of faults is related to historical evolution, so some scholars predict the possibility of fault activation by analyzing the historical evolution of faults [29,30]. The farthest period can be traced back to the penultimate Glacial period for analysis [31,32], and some scholars have assessed the risk of fault reactivation through hundreds of years of historical data on the mine [33]. Hong et al. [34] even determined the time of fault activation by measuring the age of fault rocks. Molina et al. [35] used integral transformation technology and pressure derivative to estimate the occurrence time of fault reactivation. Clendenin et al. [36] studied a fault in the southeast of Missouri. Through surveying and mapping, they showed that the Grace Corner fault zone also has a complex history of polyphase reactivation, involving three Paleozoic reactivation periods of Late Ordovician, Devonian, and Post Mississippi.

With the rapid development of computers in the 21st century, the development of numerical simulation technology is relatively mature, so many scholars have conducted some research on fault activation in the process of deep mining through various numerical simulation software. Guo et al. [37–39] revealed the fault activation mechanism attributed to successive deep mining through numerical simulation and field monitoring. Ghosh et al. [40] detected geologic structure stress states such as faults in the Rajendra underground coal mine in India to realize safer mining operations and obtain an understanding of the changes in stress distribution. Li et al. [41] researched the mechanical mechanism of fault activation through three-dimensional numerical tests and microseismic monitoring. Zuo et al. [42] studied the distance between the working face and the maximum displacement of the fault plane when the fault is activated combined with the digital speckle correlation method, discontinuous deformation method, and numerical simulation method. Taking the Barapukuria coal mine in Bangladesh as the research background, Islam et al. [43] employed the boundary element method (BEM) to research the characteristics of stress as well as deformation around the fault and the influence of groundwater on fault activation. Sainoki and Wei et al. [44,45] based on the secondary development feature of the finite difference program FLAC 3D, investigated the effects of stress wave, fault surface roughness, and other parameters on fault activation. Lv et al. [46] established a thermal water mechanical damage coupling model (THMED) with faults based on FLAC 3D. Analysis and research of the fault activation barrier effect. Haddad et al. [47] used a three-dimensional, fully

coupled porous elastic finite element simulation to evaluate the possibility of reactivation of barrier normal fault under normal fault stress state in different production scenarios

No matter through numerical simulation, indoor experimental research, or theoretical analysis, it is inevitable that some simplifications will be made to the real situation on the spot. Combined with the actual situation of the site, the analysis of fault activation can maximize the reliability of the results. In order to avoid the influence of fault activation on the mining safety of underground mines, Islavath and Liu et al. [48,49] not only established a complete monitoring system for fault activation in the underground, but also analyzed the safety of goaf near the fault during longarm mining through practical cases. Van Balen and Delogkos et al. [50,51] studied the possibility of fault reactivation based on the field activities of the Rohr Valley Rift System (RVRS) fault and the normal fault exposed by Kardia lignite mine in the Ptolemy basin, northwest Greece, respectively.

To sum up, although predecessors have carried out a great deal of fruitful studies on fault activation patterns and mechanisms under mining influence, however, there are still some deficiencies in the existing research results. First, in the past, there was much research regarding the activation of faults induced by coal extraction, while relatively little research regarding the activation of faults induced by metal mine extraction. As we all know, the deposit of metal and coal have different occurrence states and mining methods, so the fault activation effect and disaster mechanism caused by mining are also different. Second, the barrier effect of rock mass movement caused by faults is not clearly understand, which will lead to the unreasonable design of underground mine shafts and roadway engineering, resulting in the abandonment of some shaft and roadway engineering, and will significantly affect the safe, effective, and environmentally friendly mining of mines. In China, the safety production of metal mines still maintains a severe situation. On the premise of advocating safe and efficient production, it is vital to do research on the related problems faced in the mining process of underground metal mines. Therefore, based on the key factors such as the distance between the fault and the mining area, the buried depth of the fault of the upper boundary, the fault dip angle, the size of the mining area, and the fault fracture zone thickness, this paper studies the fault activation and its influencing factors on the barrier effect of rock mass movement under the influence of mining.

2. Analysis of the Fault Activation and Its Influencing Factors on the Barrier Effect of Rock Mass Movement under the Influence of Mining

If there is a fault in the surrounding rock of the mining area, it will affect the characteristics of the stress field and displacement field caused by excavation, thus causing changes in the potential energy of the rock mass within a certain range. In the process of this change, the work done by the rock mass's own gravity, on the one hand, is consumed in the friction action and slip deformation of the fault, and at the same time, it causes the discontinuous distribution of the displacement field and stress field of the rock on both sides of the fault. On the other hand, it also causes the surrounding rock in the excavation area near the fault to have the characteristics of large displacement and high-stress difference, so that the overall geometric and physical symmetry is destroyed. On the contrary, various influencing factors in the process of underground mining will also cause rock mass movement, destruction, deformation, etc., which will cause the dislocation of originally stable faults, which is called "fault activation." It is found that in the process of large-scale underground mining, faults distributed within the mining influence range will become barriers for rock mass movement, deformation, and mining stress transmission, and many adverse underground phenomena are related to this barrier mechanism. Therefore, this paper studies the factors affecting fault activation and its barrier effect. The strength of fault activation and its barrier effect on rock mass movement is mainly determined by several key factors, such as the distance (location) from the fault to the mining area, the fault's buried depth of the upper boundary, the fault dip angle, the size of the mining area and the fault fracture zone thickness.

A large three-dimensional discrete element numerical simulation software 3DEC is used in the model calculation of this paper. The size of the numerical calculation model is 1600 m along the X direction, 50 m along the Y direction, and 800 m along the Z direction. The model is divided by a regular tetrahedron grid. In order to ensure the calculation accuracy, the grid around the fault and the mining area has been densified. The entire model is divided into 688,719 grids, the maximum side length of the model grid is about 9 m, and the minimum side length is about 1 m. Since the minimum excavation size is 50 m × 100 m, according to the trial calculation result and previous calculation experience, the accuracy of the model grid can meet the calculation requirements. During the calculation, the horizontal displacement is constrained on both sides and the front and rear boundaries of the model, the bottom boundary of the model is constrained to all displacement, and the upper boundary of the model is a free surface. The parameters of numerical simulation calculation are shown in Table 1 [52].

Table 1. Parameter table of Numerical simulation calculation.

Lithology	Density ρ (g/cm^3)	Shear Stiffness (GPa)	Normal Stiffness (GPa)	Tensile Strength σ_t (MPa)	Cohesion c (MPa)	Internal Friction Angle φ (°)	Elastic Modulus E (GPa)	Poisson's Ratio
surrounding rock	2.70	/	/	1.50	1.0	38	13.06	0.269
fault plane	/	0.6	0.260	0.4	0.2	20.0	/	/
fault zone	2.20	/	/	0.1	0.1	28.0	0.6	0.260

2.1. The Evolution Law of the Influence of Mining Area Location on Fault Activation

The relative position relationship between fault and mining area generally has three situations: the mining zone is situated on the fault footwall, within the fault hanging wall, or runs through the mining zone. The calculation model and geometric parameters of the mining area are shown in Figure 1a, where L represents the distance between the fault and the mining area, taking 30 m, 60 m, 90 m, 120 m, and 150 m respectively; when the distance of 0 m from the mining area, it means that the fault cuts into the mining area.
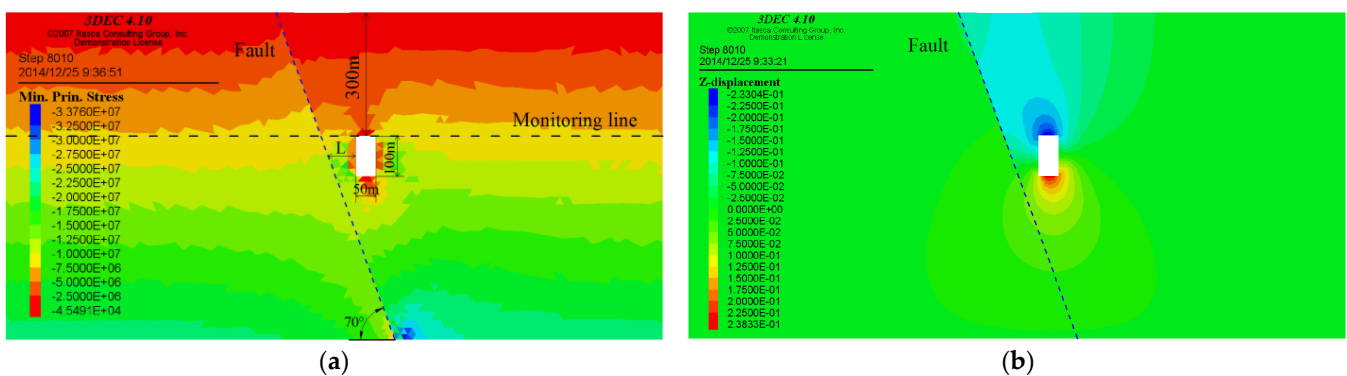

(**a**) (**b**)

Figure 1. Nephogram of stress and displacement distribution of surrounding rock when the mining area is 60 m away from the fault hanging wall, they should be listed as: (**a**) Maximum principal stress nephogram; (**b**) Vertical displacement nephogram.

2.1.1. Analyse of the Barrier Effect of Fault on Rock Mass Movement

Figures 1 and 2 respectively show the maximum principal stress distribution and vertical displacement distribution in the surrounding rock at 60 m from the footwall and hanging wall of the fault; Figure 3 illustrates the maximum principal stress distribution and vertical displacement distribution in the surrounding rock for 0 m distance between the mining zone and the fault (the fault cuts into the goaf); Figures 4 and 5 are line charts of the distribution of vertical displacement and horizontal displacement of surrounding

rock of the monitoring line under the conditions of different distances from the mining area to the fault. The calculation results indicate that the primary effects of the fault barrier's strength change are as follows. ① When the mining area is within the hanging wall of the fault. The horizontal displacement, vertical displacement, and stress field distribution on the monitoring line are continuous when the fault is far from the mining area of effect. When the fault is located in the influence range of mining, the existence of faults breaks the continuity of the displacement field and stress field distribution, as well as the barrier effect of the fault on rock movement, begins to appear. As the distance between the mining area and the fault becomes closer, the rock mass stress concentration between the fault and the goaf will steadily rise, resulting in the larger displacement difference and stress difference of the rock mass on either side of the fault, the sharp increase of the growth rate of the slip amount after the fault activation, the fault barrier effect to the displacement field and stress field of grows notably, and the degree of fault activation grows; ② When the fault cuts into the mining area, the stress concentration on the side close to the goaf is the highest, the displacement difference of the rock mass on either side of the fault on the monitoring line reaches the maximum, and the slip amount of the fault increases sharply, indicating that the fault is most likely to undergo activation and unstable slip under this working condition. The rapid growth of fault slip may induce the occurrence of rock burst under certain conditions; ③ When the mining area is situated at the fault footwall. With the decrease of the distance from the mining area to the fault, the horizontal displacement difference as well as vertical displacement difference at faults of the monitoring line increase. The increase of horizontal displacement is greater than that of vertical displacement, but the increase is not large, which is significantly smaller than the increase of slip at the fault after the fault hanging wall is mined.
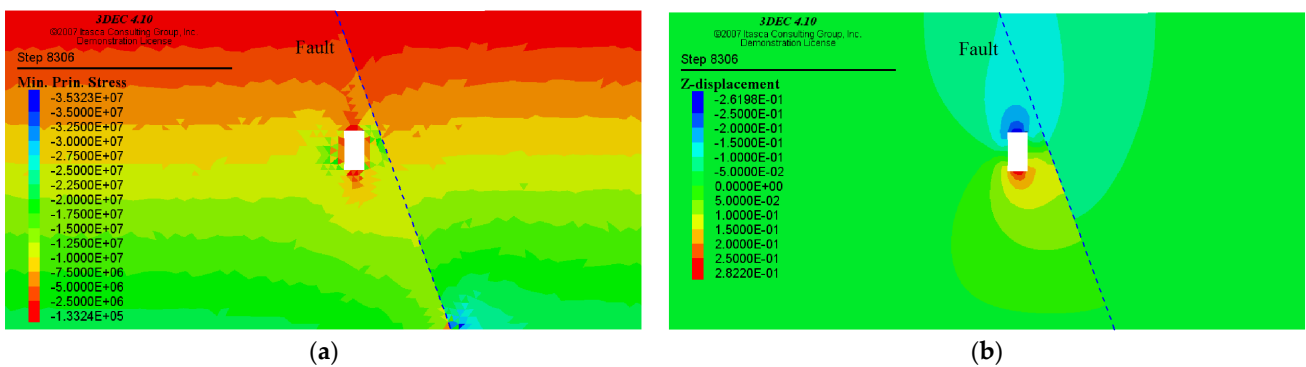

(**a**)   (**b**)

Figure 2. Nephogram of stress and displacement distribution of surrounding rock when the mining area is 60 m away from the fault footwall, they should be listed as: (**a**) Maximum principal stress nephogram; (**b**) Vertical displacement nephogram.

(**a**)   (**b**)
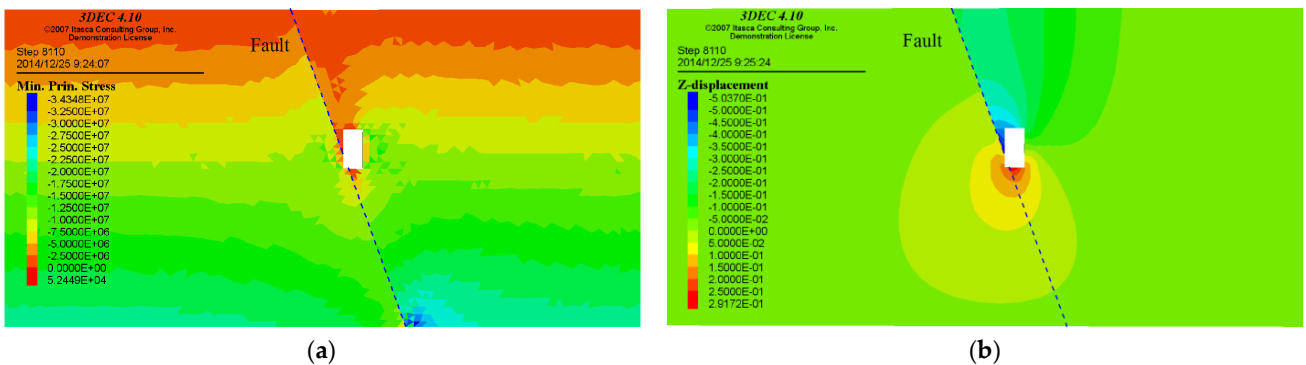
Figure 3. Nephogram of stress and displacement distribution of surrounding rock when the mining area is 0 m away from the fault (the fault cuts into the goaf), they should be listed as: (**a**) Maximum principal stress nephogram; (**b**) Vertical displacement nephogram.
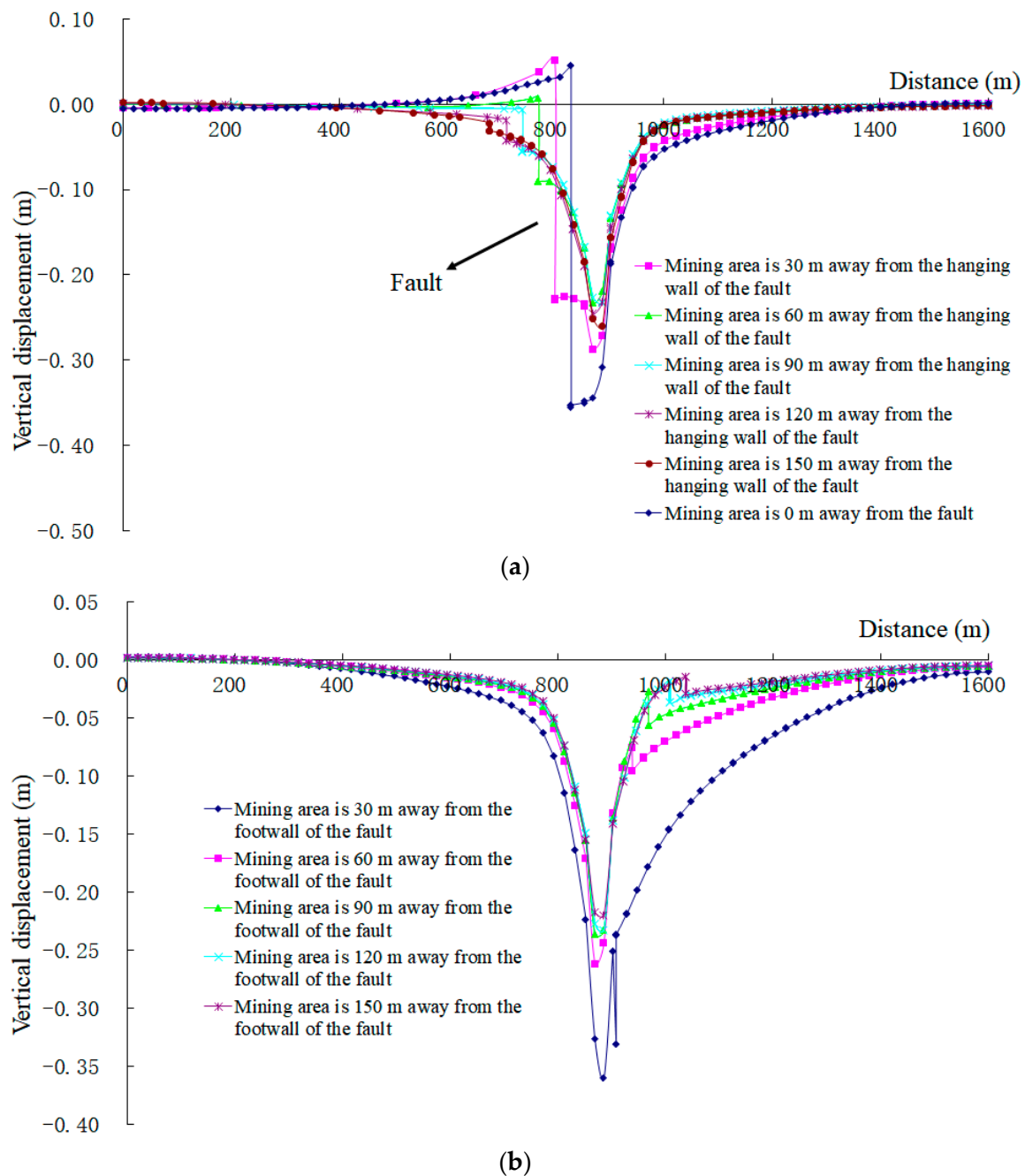
Figure 4. Line chart of vertical displacement distribution of surrounding rock on monitoring line at different distances from the mining area to the fault, they should be listed as: (**a**) The mining area is located in the fault hanging wall; (**b**) The mining area is located in the fault footwall.

In case the distance of the mining area from the hanging wall and footwall is the same, mining in the fault hanging wall will results in a notable growth in the discontinuity of the displacement field and stress field compared to mining in the fault footwall, as well as a much stronger confining pressure relief effect of surrounding rock, suggesting that it is simpler to activate the fault while the mining area is situated in the hanging wall of the fault. Fault activation is most likely to occur when the fault cuts into the mining area and induces the occurrence of a rock burst.
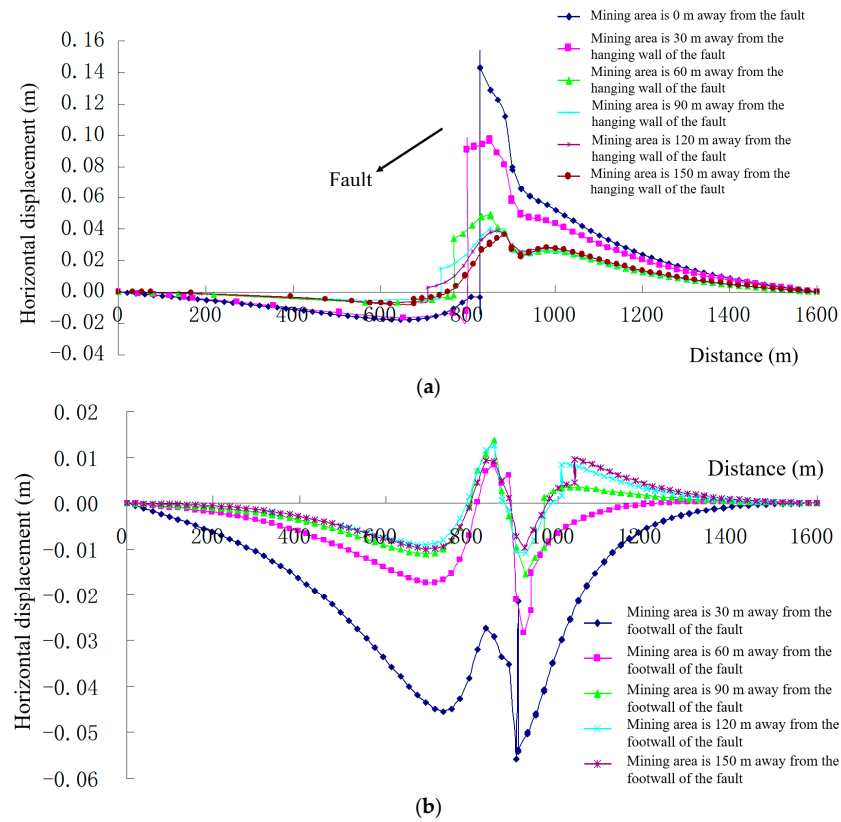
Figure 5. Line chart of horizontal displacement distribution of surrounding rock on monitoring line at different distances from the mining area to the fault, they should be listed as: (**a**) The mining area is located in the fault hanging wall; (**b**) The mining area is located in the fault footwall.

2.1.2. Analysis of the Stress Change of Fault Plane Caused by Mining

Figures 6 and 7 show the normal stress and shearing stress distribution on the plane of the fault at different distances to the fault hanging wall within the mine area, respectively. As can be seen, the additional shearing stress and normal stress are produced on the fault plane due to the effect of mining, which changes both normal stress and shearing stress. The shear stress to normal stress ratio is greater, the fault is activated more easily. This is due to the possible increase in shear stress and decrease in normal stress under the influence of mining, resulting in shearing stress surpassing the shear strength.
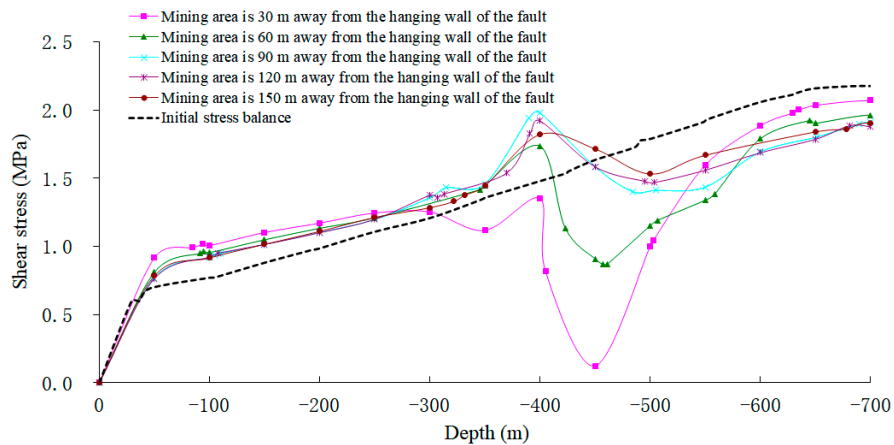

Figure 6. When the mining area is situated within the fault hanging wall, the shear stress distribution on the fault plane is at various locations.
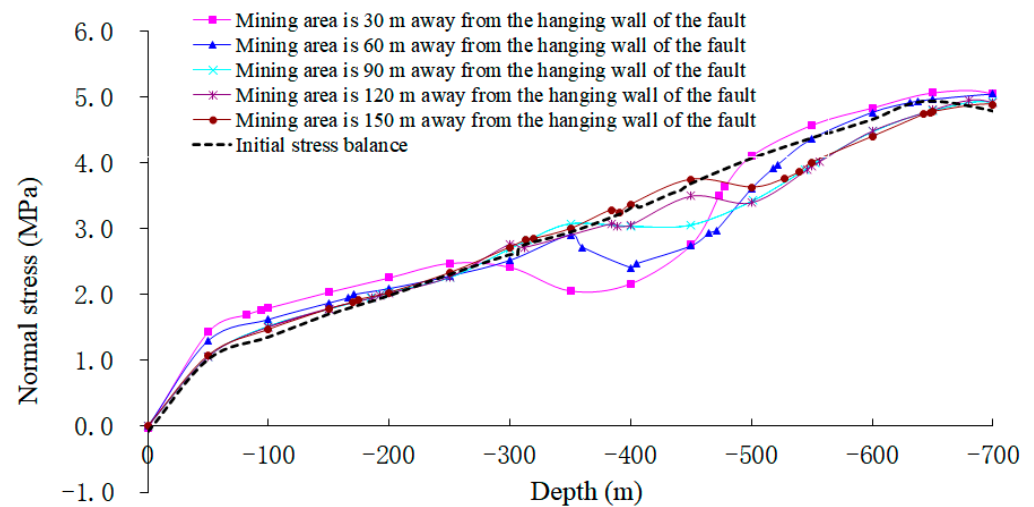
Figure 7. When the mining area is situated within the fault hanging wall, the normal stress distribution on the fault plane is at various locations.

The major features of shearing stress distribution when excavating fault hanging walls are listed below. ① Within the depth of 0 to −400 m, the additional shear stress is positive. the shearing stress reduces in parallel with the increment of the mining zone distance to the fault, making it less likely that the fault will be activated. The additional shear stress reaches its maximum at a depth of −70 m. For example, the largest value of additional shear stress is 0.259 MPa at 30 m from the mining region to the fault hanging wall which decreases linearly downward. The normal tensile stress increases significantly again until the extrusion area appears. This is consistent with the reason that excavation causes the shallow opening and sliding of fault hanging wall and the center of gravity downward enhances the compression of the lower unpulled fault plane; ② In the depth range of −400 m to −700 m, the shearing stress on the fault plane increasingly differs from the shearing stress at initial equilibrium as the distance between the excavation area and the fault decreases. The additional shearing stress is negative. The progressive reduction in shear stress may contribute to the progressive decline in the probability of fault activation. The Coulomb–Mohr criterion [53] and the Byerlee fault slip criterion [54] both state that the fault has not undergone activation dislocation within this depth range.

The normal stress distribution exhibits the following primary characteristics during the excavation of the hanging wall of the fault. ① Between 0 m and −300 m in depth. Additional tensile stresses are essentially absent when the fault plane is more than 90 m from the mining zone. but when it is less than 60 m, a slight increase in normal stress; ② Between −300 m and −700 m in depth. The additional tensile stress is negative, as well as decreasing with the distances between the excavated area and the fault, the maximum value of additional tensile stress tends to move to the bottom left of the goaf. The reason being that the vertical distance from the lower left of the goaf to the fault is nearest, and after excavation and unloading, there is significant additional tensile stress in the fault plane.

Figures 8 and 9 depict the normal stress and shearing stress distribution on the fault plane for various distances from the mining area. It can be seen that the main characteristics of the shearing and the normal stress distribution are as follows. ① Additional shear stress is negative in the depth range from 0 to −100 m. When the fault plane is farther away from the extraction area, the shearing stress reduces and the normal stress rises on the fault plane; ② the additional shear stress is negative between −100 and −400 m deep. As the excavation area becomes closer to the fault, the maximum additional shear stress progressively grows, while the shearing stress gradually decreases. In contrast, the additional normal stress is negative as well as the normal stress gradually decreases. The peak value of added tensile stress steadily rises with the distance reduction from the excavation area to the fault, and there is a tendency to approach the top right of the goaf. The fault is activated more readily

the weaker the shear strength on the fault plane is; ③ Within the depth range of −400 m to −700 m. When the footwall of the fault is excavated, the impact on the fault below the goaf's bottom depth is minimal, as evidenced by the fact that the normal stress and shear stress alter little with depth.
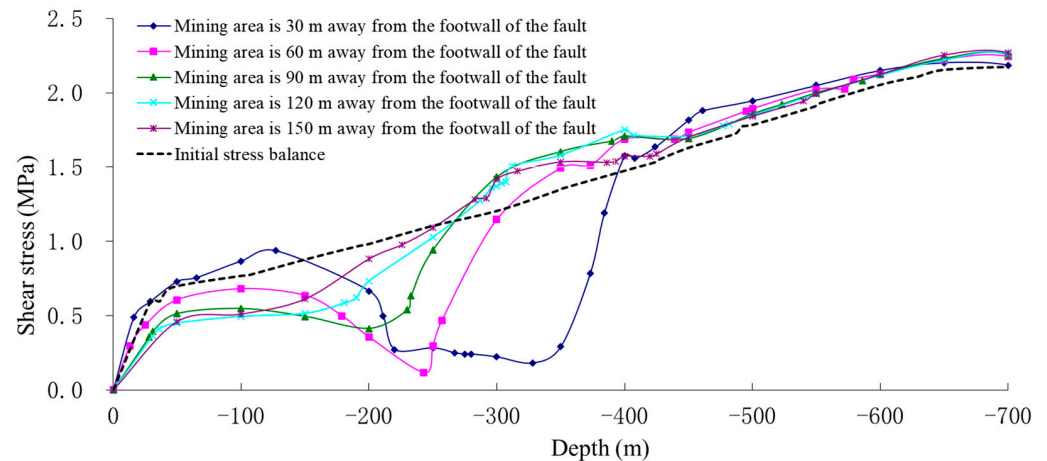

Figure 8. When the mining area is situated within the fault footwall, the shear stress distribution on the fault plane is at various locations.
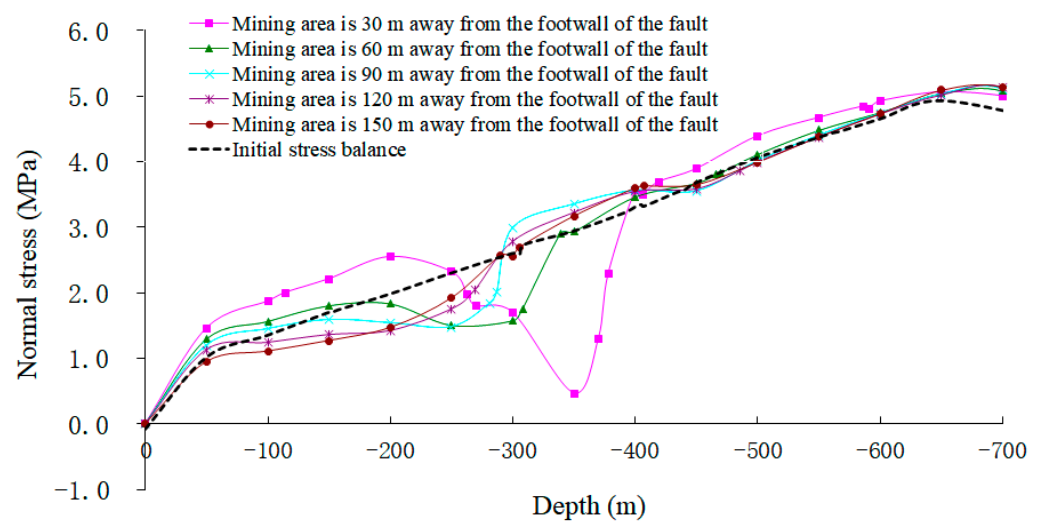

Figure 9. When the mining area is situated within the fault footwall, the normal stress distribution on the fault plane at various locations.

Based on the previous analysis, the effect mechanisms of varying excavation area distance to the fault on the fault plane's shearing stress and fault activation can be summarized. ① Shearing stress progressively reduces as the fault plane is further away from the extraction area, so does the normal stress, and the reduction in normal stress significantly outweighs the decline in shearing stress. In accordance with the sliding criteria of fault, i.e., the shearing stress to normal stress ratio becomes larger. Therefore, It is simpler to cause fault activation the closer the excavation area is to the fault; ② Along with the reduction of the mining area distance to the fault when excavating the fault footwall, the added tensile stress progressively increases, as does the ratio that is additional tensile stress versus the additional shearing stress, i.e., the easier it is to activate the fault, the greater the shear stress/normal stress. In other words, whether the fault hanging wall or footwall is exploited, it is simpler to cause fault activation the closer the mining area is to the fault.

2.2. Analysis of the Evolution Law of the Impact of Upper Boundary Buried Depth on Fault Activation

The numerical geometric model in Figure 1 is reflected the thickness H of the rock layer above the upper border of the model is altered, taking into account the impact of the buried depth of the upper boundary of the fault on its activation. The buried depth H in this study is assumed to be 200, 300, 400, 500, 600, and 700 m, respectively, and the corresponding mining depths are 600, 700, 800, 900, 1000, and 1100 m. The distance between the mining area and the fault L is considered to be 60 m, using the hanging wall mining of the fault as an example.

2.2.1. Statement of the Barrier Effect of Fault on Rock Mass Movement

The distribution law of the displacement field of the surrounding rock at the monitoring line under different conditions of the burial depth of the upper boundary of the fault, as shown in Figure 10. The existence of the fault destroys the continuity of the displacement field. The displacement of the monitoring line shows a step-like abrupt increase change at the fault. The distribution of vertical displacement and horizontal displacement is obviously blocked by the fault near to the goaf on the side of the hanging wall. As the burial depth increases, the larger the displacement difference between the two sides of the fault, the larger the slip of the fault. When the burial depth is 200 m, the vertical displacement difference and horizontal displacement difference between the surrounding rocks on both sides of the fault are 0.347 m and 0.128 m separately. When the burial depth increases to 700 m, the vertical displacement and horizontal displacement difference increase to 1.779 m and 0.660 m separately, this demonstrates that the fault barrier impact on the displacement field grows with the depth at which its upper border is buried.
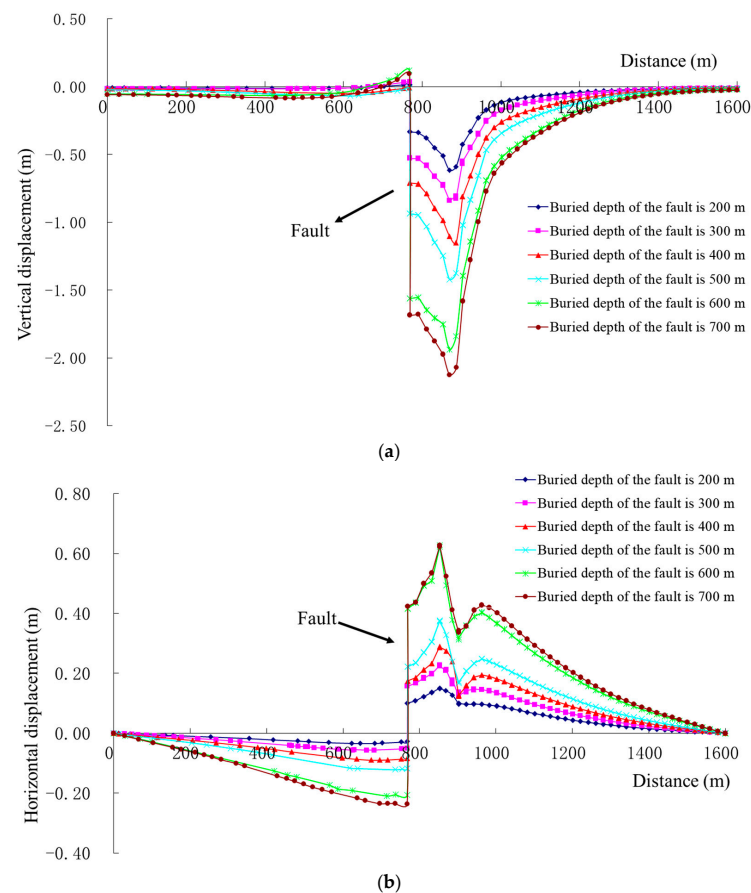

Figure 10. Displacement distribution of surrounding rock of the monitoring line under the condition of different upper boundary buried depths of the fault, they should be listed as: (**a**) Vertical displacement distribution; (**b**) Horizontal displacement distribution.

2.2.2. Statement of the Tress Change of Fault Plane Caused by Mining

Figure 11 depicts the shear stress distribution on the fault plane for various fault upper boundary burial depths. It can be seen that the influence of the upper boundary burial depth on the fault activation is mainly manifested in: ① When the upper boundary burial depth of the fault is different, the shear stress value that is different on the same fault plane. With the rising of burial depth, the shear stress value also increases, and the peak value of shear stress also increases. For instance, when the burial depth increases from 300 to 700 m, the peak value of shear stress increases from 2.48 to 4.75 MPa. This law shows that the deeper the mining goes to the stratum, the shear stress on the fault plane increases with mining influence, making the fault easier for it to become activated. ② The change in mining depth will not change the shear stress distribution law on the fault plane (Figure 11). When other parameters are fixed, the shear stress distribution and peak value position are the same under varied mining depths, that is, the shear stress increases to its greatest between 0 and −50 m of depth, progressively declines between −50 and −300 m, and is influenced by mining between −300 and −400 m of depth because it corresponds to the orebody mining height. Within the depth range of −400 to −500 m, the shear stress progressively reduces.
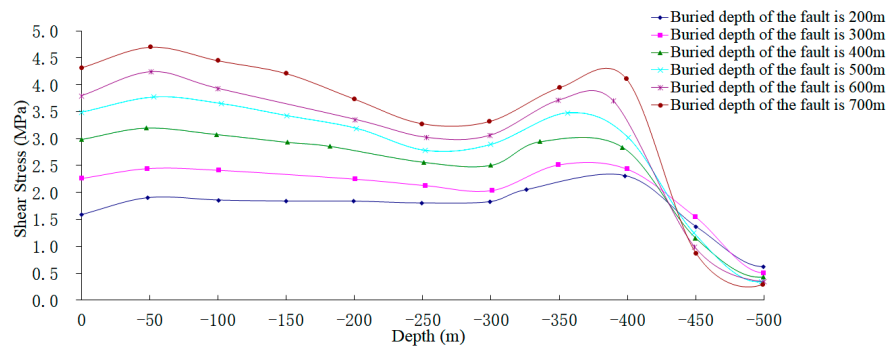

Figure 11. The shear stress distribution of the fault plane under various buried depths of the upper boundary of the fault.

The principal stress difference distribution of fault hanging wall rock at the intersection of the monitoring line and the fault under the conditions of different upper boundary burial depths of the fault, as shown in Figure 12. The maximum and minimum principal stresses in the hanging wall of the fault are larger than those in the footwall, and the difference between the maximum and minimum principal stresses grows with the upper boundary burial depth of the fault, showing that the fault contributes to a greater barrier effect on stress field propagation.
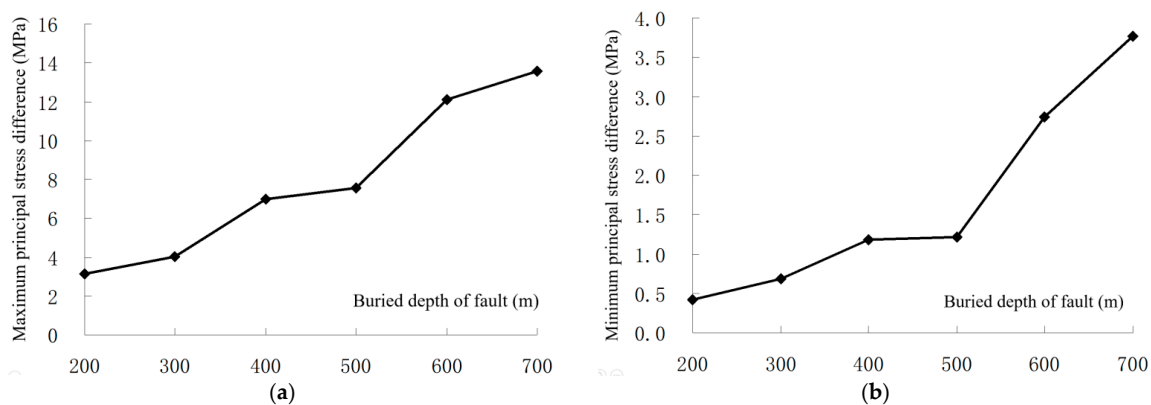

Figure 12. The distribution of stress difference between the hanging wall and footwall of surrounding rock on the monitoring line under different upper boundary burial depths of fault, they should be listed as: (**a**) Maximum principal stress difference; (**b**) Minimum principal stress difference.

2.3. Study on the Influence of Fault Dip Angle on Fault Activation

To analyze how the fault dip angle affects the fault activation, this paper considers the situation when the fault cuts into the mining area, the numerical geometric model schematic diagram is shown in Figure 13a, in which α is the fault dip angle, the intersection A of the fault and the mining area left boundary serves as the monitoring point, and the fault dip angle α is determined to be 30°, 40°, 50°, 60°, 70°, and 80°, respectively.
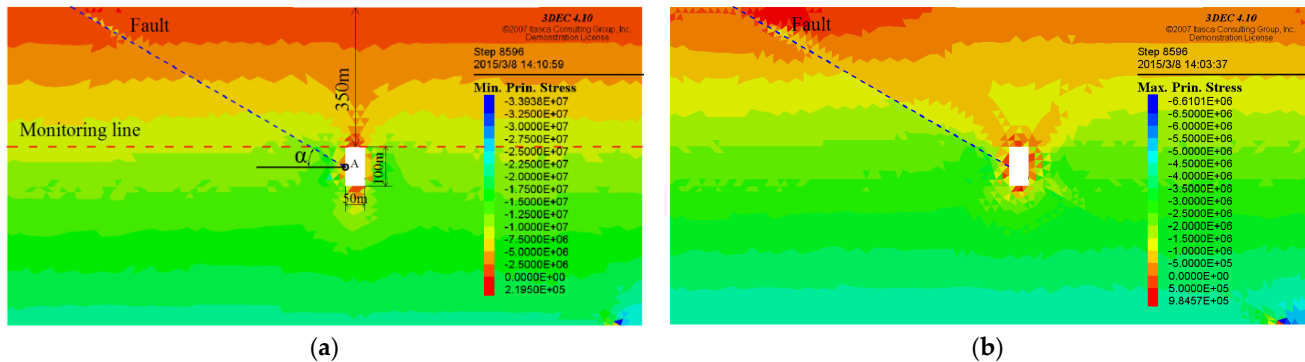

(**a**)   (**b**)

Figure 13. Stress field distribution of surrounding rock on the fault plane when the fault dip angle of 30°, they should be listed as: (**a**) Maximum principal stress distribution; (**b**) Minimum principal stress distribution.

2.3.1. The Expound of the Barrier Effect of Fault Dip Angle on Rock Mass Movement

Space being limited, only the stress field distribution of the surrounding rock around the fault is shown with the fault dip angle is 30° and 80° (Figures 13 and 14). The stress concentration in the fault hanging wall in the mining area on both sides of the rock grows with the fault dip angles increase. The tensile stress is mainly near monitoring point A, and its value is increasing. Figure 15 shows the displacement distribution of vertical and horizontal surrounding rock along the monitoring line of different fault dip angles, and Figure 16 shows the slip amount of the fault at monitoring point A of different fault dip angles. As the fault dip increases, the results show that the difference in rock mass displacement on the fault plane on both sides gradually increases, and the vertical displacement difference and horizontal displacement difference of the surrounding rocks on the fault footwall and hanging wall of the monitoring line gradually increases, the barrier effect of fault plane on displacement gradually increases. The slip amount at the junction point A of the fault and the mining area is the largest, and the slip amount at point A increases practically linearly as the fault dip angle rises, indicating stress and displacement fields are significantly impacted by the barrier effect of the fault.
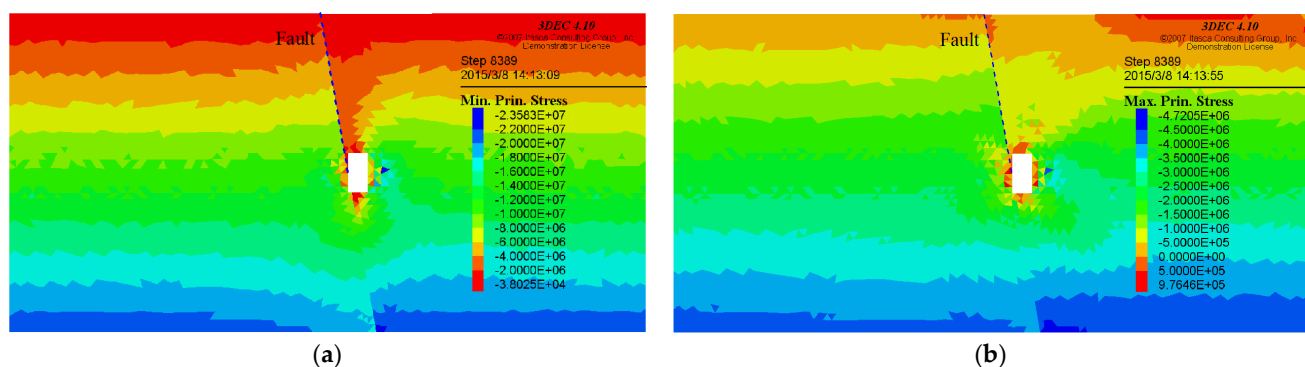

(**a**)   (**b**)

Figure 14. Stress field distribution of surrounding rock on the fault plane when the fault dip angle of 80°, they should be listed as: (**a**) Maximum principal stress distribution; (**b**) Minimum principal stress distribution.
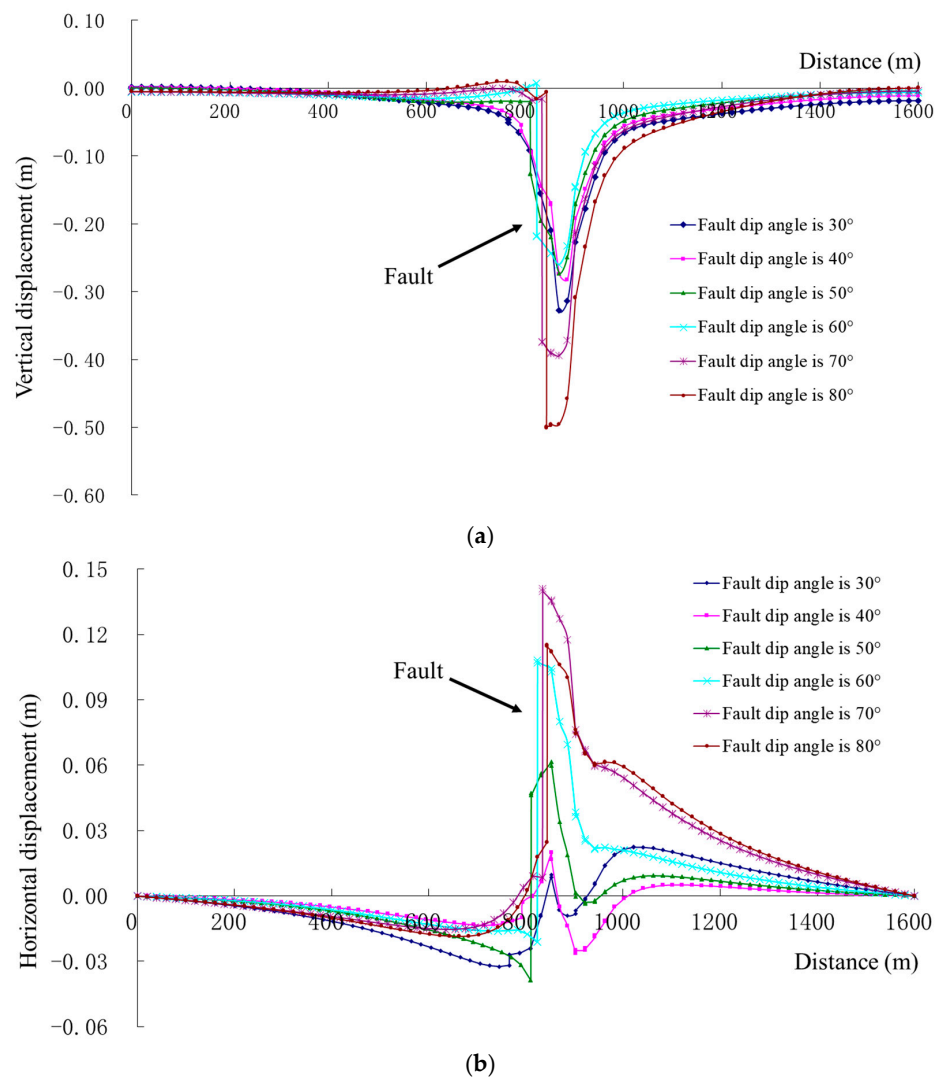
(**a**)

(**b**)

Figure 15. The displacement distribution of surrounding rock along monitoring lines of different fault dip angles, they should be listed as: (**a**) Vertical displacement distribution; (**b**) Horizontal displacement distribution.
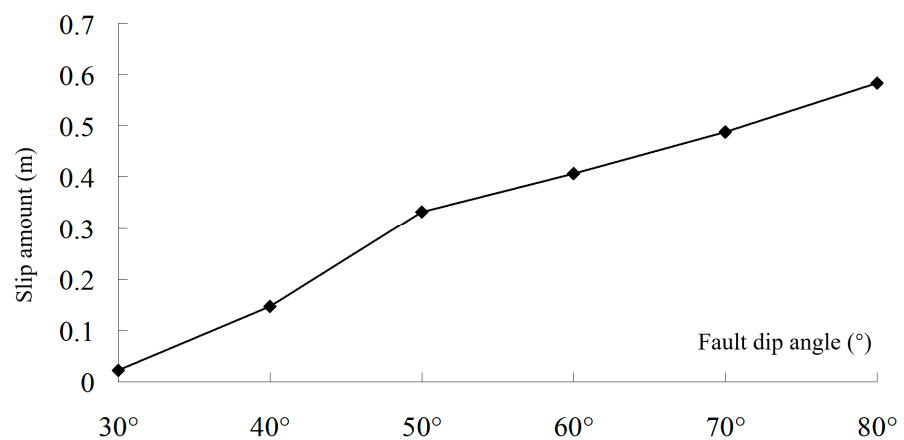

Figure 16. The shear stress distribution at the fault plane under various buried depths of the upper boundary of fault.

2.3.2. The Expound of the Stress Change on Fault Plane Caused by Mining

Figure 17 displays the shear stress to normal stress ratio distribution along the fault plane at various fault dip angles ($30° \leq \alpha \leq 80°$) during the downward excavation of the fault hanging wall. The calculation results show that as the fault dip angle increases, the ratio of shear stress to positive stress becomes larger and larger, demonstrating that the fault is easier to activate. For various fault dip angles, the shear stress and positive stress ratio distribution are consistent, which in the range from 0 m to −50 m depth increases sharply to the peak, and then gradually decreases and stabilizes. For example, the maximum value of shear stress to normal stress ratio is from 0.79 to 0.66 as the fault dip angle from $\alpha = 80°$ to $\alpha = 50°$.
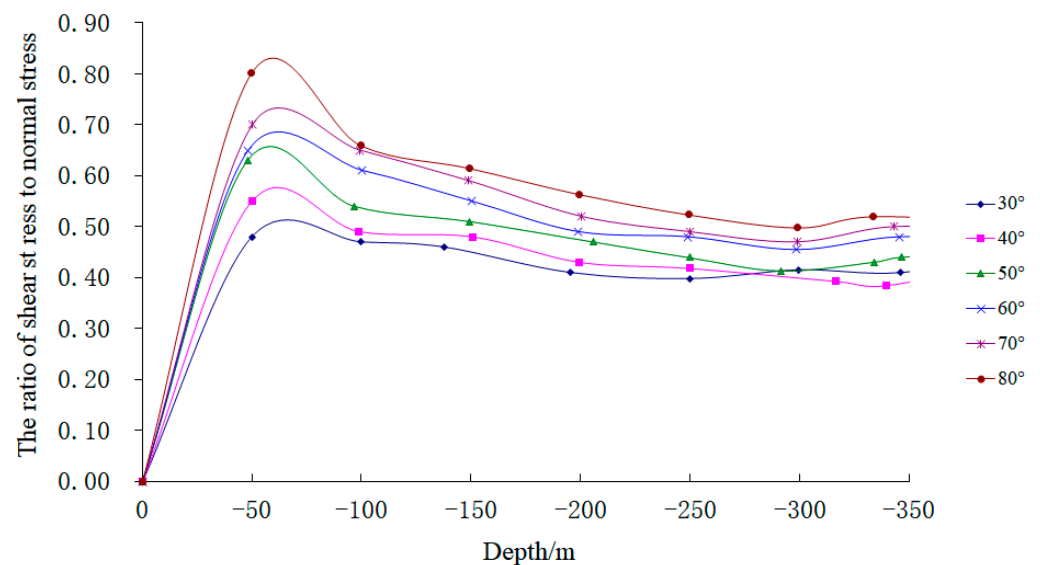

Figure 17. The shear stress to normal stress ratio distribution on the fault plane at various fault dip angles.

2.4. *The Analysis of the Impact of Mining Size on Fault Activation*

In order to study the influence of mining size on fault activation and its barrier effect on rock mass movement, different mining sizes L were analyzed, which is reflected in the numerical geometric models shown in Figures 18a and 19a, that is, the difference in L. In this paper, L is taken as 100, 200, and 300 m, corresponding to the mining sizes of 50 m × 100 m, 50 m × 200 m, 50 m × 300 m, 100 m × 50 m, 200 m × 50 m, and 300 m × 50 m respectively, taking only the mining of the hanging wall of the fault as an example.

(**a**) (**b**)

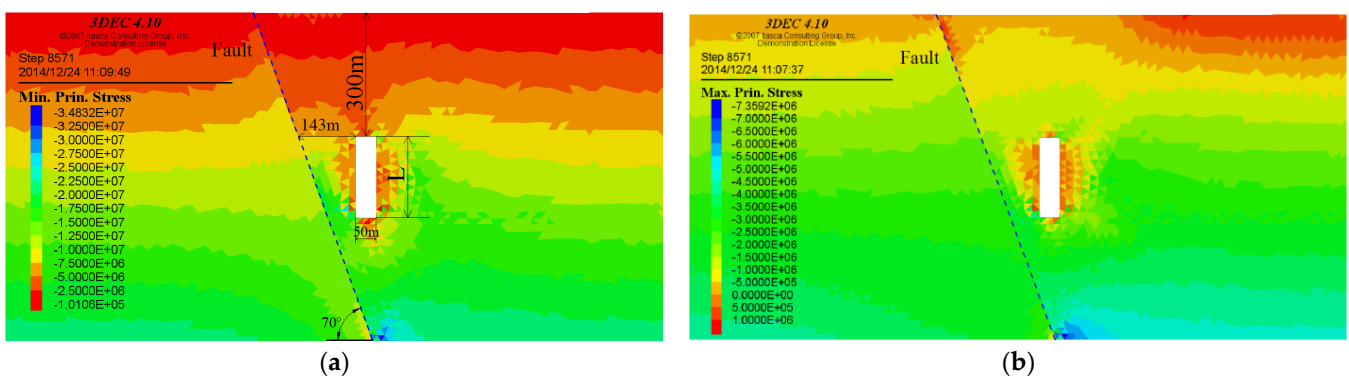**Figure 18.** The stress field distribution in the surrounding rock at the excavation size of 50 m × 200 m, they should be listed as: (**a**) Maximum principal stress distribution; (**b**) Minimum principal stress distribution.
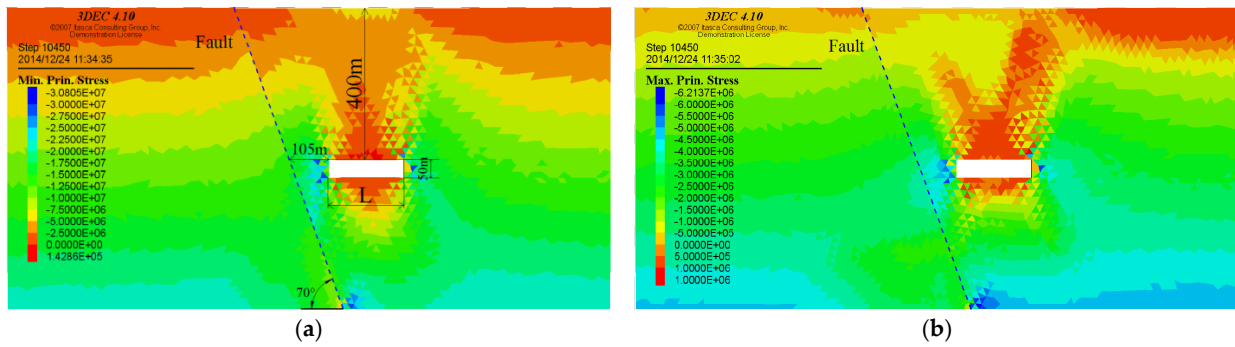
Figure 19. The stress field distribution in the surrounding rock at the excavation size of 200 m × 50 m, they should be listed as: (**a**) Maximum principal stress distribution; (**b**) Minimum principal stress distribution.

2.4.1. Analysis of Barrier Effect of Mining Size on Rock Mass Movement

As the depth and mining size becomes greater, the barrier degree of the fault plane is enhanced, and the maximum displacement value of the surrounding rock on the hanging wall near the fault plane increases dramatically. When the mining size increases along the vertical direction, the displacement difference between the rock masses on both sides of the fault plane will also have a positive correlation change, and the stress value and the maximum principal stress concentration will also increase. When the vertical direction of mining size changes to 50 m × 100 m, 50 m × 200 m, 50 m × 300 m, the corresponding displacement difference changes are 0.06 cm, 0.35 cm, and 2.52 m. When the mining size changes along the horizontal direction, it also presents the same change law as the vertical direction. When the mining size changes along the horizontal direction are 100 m × 50 m, 200 m × 50 m, 300 m × 50 m, the corresponding displacement difference changes are 0.15 m, 0.8 m, and 1.0 m. Figure 20 illustrates the displacement field distribution of the surrounding rock under different mining sizes. Compared with the aforementioned initial excavation size, the increase in the excavation size resulted in a large discontinuous change in the displacement distribution and maximum principal compressive stress of the rock mass on both sides of the fault plane. Especially after doubling the mining depth, the displacement and the maximum principal compressive stress values of the surrounding rock in the excavation area close to the fault plane increase more year-on-year, which also indicates that the barrier effect of the fault plane has been greatly strengthened. Through comparison, it can be found that the influence of the mining area change in vertical depth direction on the barrier degree is more sensitive than the change in horizontal length direction under the condition that the mining area and fault are separated by the same distance. The influence area of rock mass movement and deformation increases with the depth of the excavation area. The more potential energy consumed by the plastic deformation of the fault plane and the friction of the structural plane, the more significant the difference in deformation of rock movement between the two sides of the fault plane.
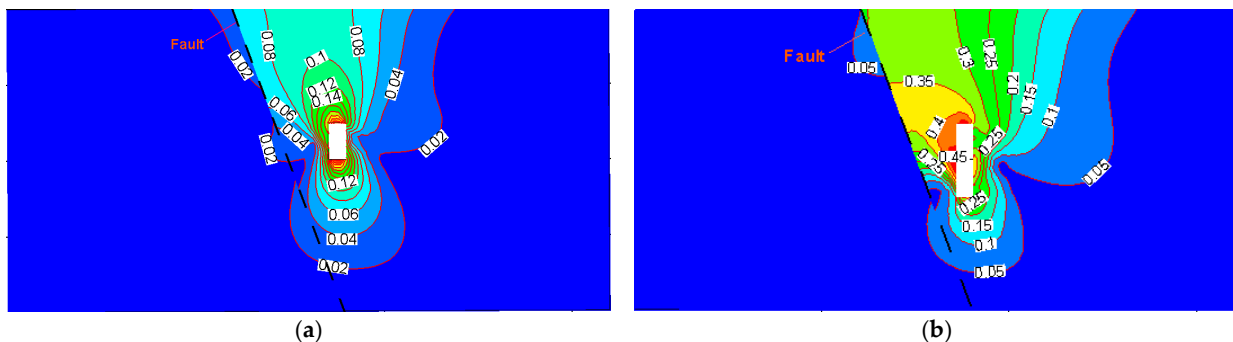

Figure 20. *Cont.*
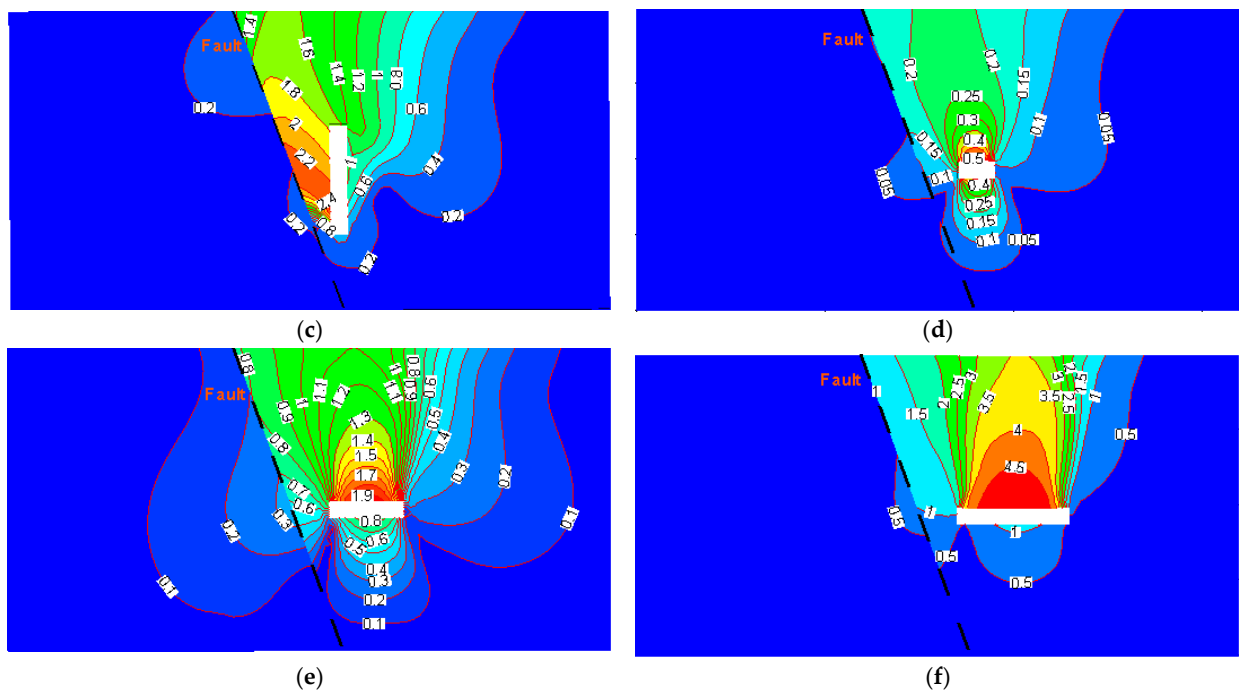
Figure 20. Absolute displacement distribution of surrounding rock under different mining sizes (unit: m), they should be listed as: (**a**) Mining size is 50 m × 100 m; (**b**) Mining size is 50 m × 200 m; (**c**) Mining size is 50 m × 300 m; (**d**) Mining size is 100 m × 50 m; (**e**) Mining size is 200 m × 50 m; (**f**) Mining size is 300 m × 50 m.

2.4.2. Analysis of the Changes in the Stress of Fault Plane Caused by Mining

The shear stresses distribution on the fault plane under various excavation sizes is depicted in Figure 21. It can be observed that the shear stress and additional shear stress rise when the distance between the mining area and the fault is fixed. Regardless of the increase in the length or height of the mining area, the possibility of fault activation also increases.
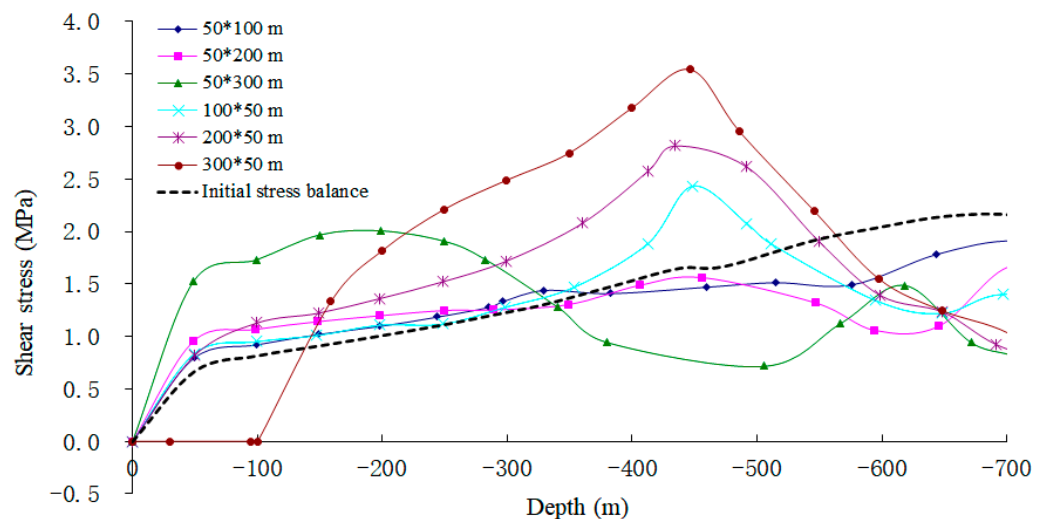

Figure 21. Shear stress distribution at the fault plane with different mining sizes.

When the mining size increases along the length direction, the shear stress distribution rule is obvious. The peak shear stress appears near the depth of −450 m, and the value increases with the increase of mining length. Such as the maximum shear stress is 2.434 MPa for a mining size of 100 m × 50 m. The maximum shear stress is 2.817 MPa when the mining size increases to 200 m × 50 m. When the mining size increase to 300 m × 50 m,

the maximum shear stress increases to 3.543 MPa near the depth of -450 m. While the shear stress that is 0 MPa in the depth range of 0 m to -100 m, demonstrating that the mining-affected fault has been pulled away near the surface.

When the mining size increases along the height direction, the shear stress increases compared with the initial equilibrium state between 0 m and -350 m deep above the goaf. Positive additional shear stress is present, and it rises with the increase of mining depth. Indicating that the larger the mining size along the vertical direction, the higher the probability of fault activation. When the mining size is 50 m $\times$ 100 m and 50 m $\times$ 200 m, the maximum shear stress near the depth of -50 m is 0.673 MPa and 0.796 MPa respectively, and when the mining size increases to 50 m $\times$ 300 m along the height direction, there is a tendency for the maximum shear stress to extend downwards, the maximum shear stress is 2.006 MPa and has a large increase. Below the depth of -350 m, the additional shear stress is negative and the shear stress decreases.

2.5. Research on the Influence Law of the Effect of Fault Zone Thickness on Fault Activation

The influence of the barrier effect of fault zone thickness on rock movement is analyzed, which is depicted in Figure 22a numerical geometric model, that is, the difference of horizontal thickness a. In this paper, the horizontal thickness of the fault fracture zone is taken as 10, 20, 30, 50, and 60 m respectively. Taking fault hanging wall mining as an example, Figure 22 depicts the length between the mining area and the fault.
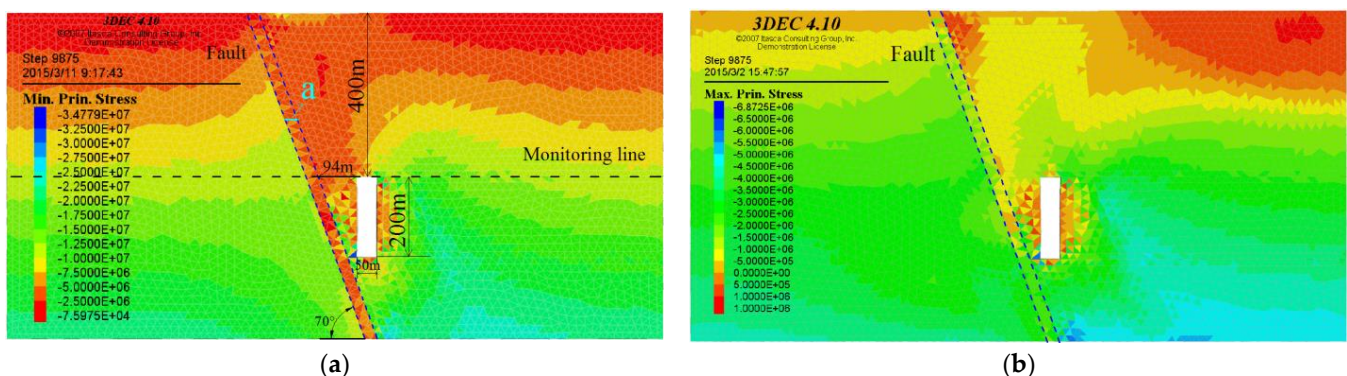

(**a**)   (**b**)

Figure 22. The principal stress distribution of surrounding rock when the thickness of the fault zone is 30 m, they should be listed as: (**a**) Maximum principal stress distribution; (**b**) Minimum principal stress distribution.

The calculated results indicate that the maximum principal compressive stress concentration degree between the mining area and the fault zone will increase, the barrier effect of the fault fracture zone on the stress field is stronger and the stress difference between the hanging wall and footwall of the fault zone is greater as the thickness of the fault fracture zone increases. When the fault zone is 30 m thick, the stress field distribution of the surrounding rock is shown in Figure 22, Figure 23 shows the displacement distribution of surrounding rock on the monitoring line with different fault zone thicknesses. The analysis shows that when the fault fracture zone thickness develops, the barrier degree of the fracture zone continually improves and the difference in displacement value of the surrounding rock on both sides of the fracture zone steadily increases. For example, when the thickness of the fault zone is 10 m, the horizontal displacement difference at the fault zone of the monitoring line is 0.414 m, and the vertical displacement difference is 1.193 m. When the fault zone thick increases to 60 m, the horizontal displacement difference of surrounding rock at the fault zone of the monitoring line increases to 0.57 m, while the vertical displacement difference increases to 1.57 m.
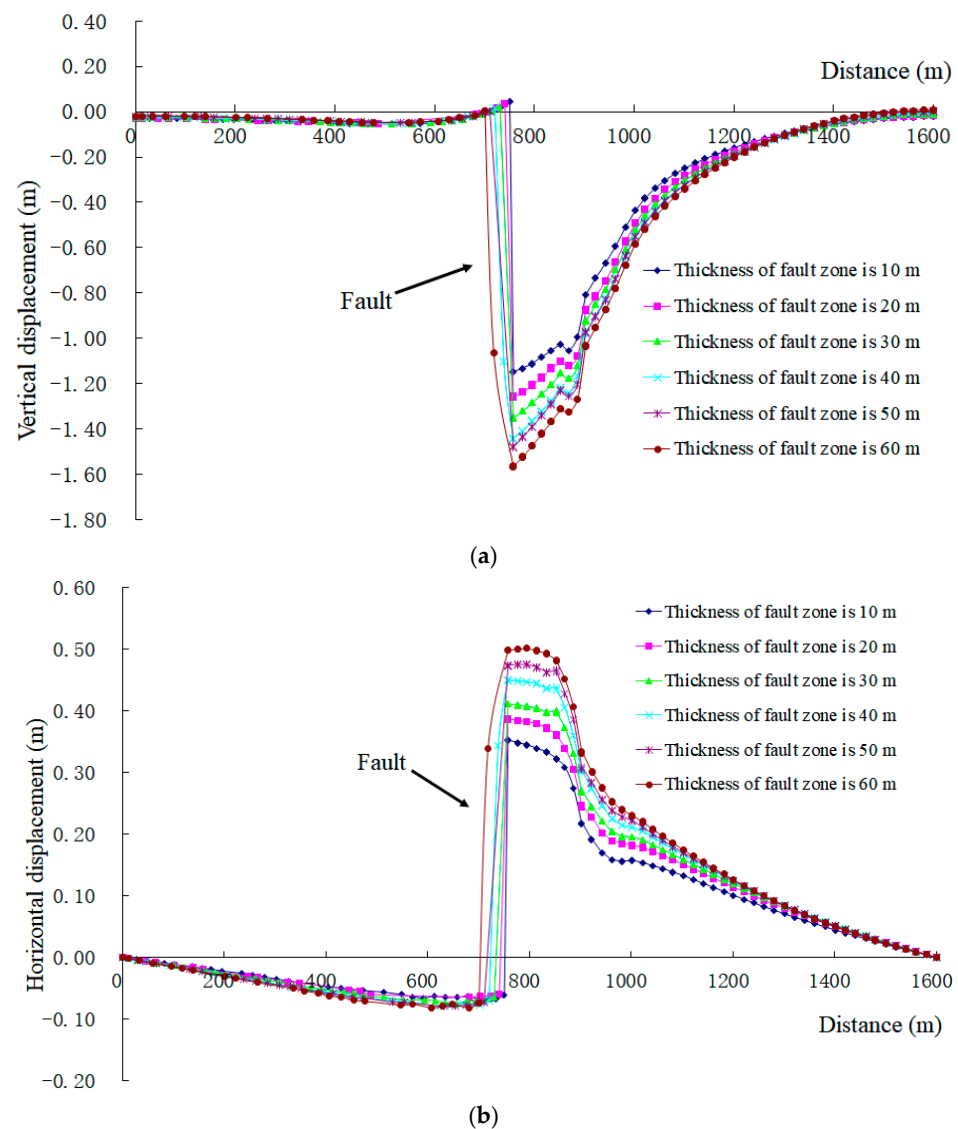
Figure 23. Displacement distribution of monitoring lines under different fault zone thicknesses, they should be listed as: (**a**) Vertical displacement; (**b**) Horizontal displacement.

3. Conclusions

(1) The stress concentration degree of the rock mass between the goaf and the fault increases gradually as the distance between them decreases. As a result, the displacement difference and stress difference of rock on two sides of the fault are becoming increasingly larger. After the fault activation, the development rate of slip amount quickly accelerates, and the fault barrier effect on the displacement field and stress field increases significantly. Excavation leads to additional shear stress and additional normal stress on the fault plane is generated, which makes the shear stress and normal stress change. An increase in shear stress or a decrease in positive stress can easily lead to a shear stress greater than the shear strength, which induces fault activation, that is, the larger the ratio of shear stress to positive stress, the more easily the fault is activated.

(2) The increasing of maximum and minimum principal stress difference as the upper bound of the fault buried depth increases. At the same time, the greater the displacement difference on both sides of the fault, the greater the slip of the fault, which indicates that the blocking effect of the fault on the propagation of the stress field also increases. The maximum value of shear stress and the value of shear stress both rise as buried depth increases. For example, maximum shear stresses range from 2.48 MPa for 300 m of buried

depth to 4.75 MPa for 700 m of buried depth. This law shows that the deeper the mining goes to the stratum, the fault is more susceptible to be activated by mining the bigger the fault plane shear stress is.

(3) The displacement difference of the rock mass on both sides of the fault plane shows a positive correlation with the increase of the fault dip angle. The same is true for the vertical and horizontal displacement difference of the hanging wall and footwall rock at the monitoring line position and the slip amount of the intersection point A between the fault and the goaf. In addition, the slip at point A shows a linear increase, which can be concluded that the barrier effect of fault on the stress field and displacement field is significantly increased. The shear stress to normal stress ratio grows as the fault dip angle increases, suggesting that the fault is more easily activated, and it is from 0 m to -50 m grows abruptly to the peak, then falls gradually and tends to remain stable. There is a constant distribution law for this ratio between shear stress and normal stress in different fault dip angles.

(4) The increase in excavation size makes the displacement distribution and the maximum principal compressive stress of both sides of the fault plane's rock mass appear discontinuous changes by a large margin. Especially after doubling the mining depth, The displacement value of surrounding rock and maximum principal compressive stress in the excavation region close to the fault plane grow year-on-year, indicating that the fault plane barrier effect has been significantly increased. When a certain distance separates the mining area from the fault, no matter whether the mining size increases in length or height, the shear stress and additional shear stress on the fault plane will increase accordingly. This raises the likelihood that the fault will be activated.

Author Contributions: Conceptualization, Y.G.; methodology, Y.G.; validation, Y.G. and L.L.; formal analysis, Y.G., L.L. and C.W.; resources, Y.G.; writing—original draft preparation, Y.G., L.L. and C.W.; writing—review and editing, Y.G., L.L. and C.W.; funding acquisition, Y.G. and C.W. All authors have read and agreed to the published version of the manuscript.

Institutional Review Board Statement: Not applicable.

Informed Consent Statement: Not applicable.

Data Availability Statement: Not applicable.

Conflicts of Interest: The authors declare no conflict of interest.

References

1. Li, P.; Cai, M.F. Challenges and new insights for exploitation of deep underground metal mineral resources. *Trans. Nonferrous Met. Soc. China* **2021**, *31*, 3478–3505. [CrossRef]
2. Cai, M.F.; Brown, E.T. Challenges in the mining and utilization of deep mineral resources. *Engineering* **2017**, *3*, 432–433. [CrossRef]
3. Cai, M.F.; Li, P.; Tan, W.H.; Ren, F.H. Key Engineering Technologies to Achieve Green, Intelligent, and Sustainable Development of Deep Metal Mines in China. *Engineering* **2021**, *7*, 1513–1517. [CrossRef]
4. Lei, G.W.; Yang, C.H.; Wang, G.B.; Chen, S.W.; Wei, X.; Huo, L. The development law and mechanical causes of fault influenced zone. *Chin. J. Rock Mech. Eng.* **2016**, *35*, 231–241.
5. Luo, H.; Li, Z.H.; Wang, A.W.; Xiao, Y.H. Study on the evolution law of stress field when approaching fault in deep mining. *J. Chin. Coal Soc.* **2014**, *39*, 322–327.
6. Lyu, P.F.; Bao, X.Y.; Lyu, G.; Chen, X.H. Research on Fault Activation Law in Deep Mining Face and Mechanism of Rockburst Induced by Fault Activation. *Adv. Civ. Eng.* **2020**, *2020*, 8854467.

7. Hu, X.Y.; Wang, L.G.; Lu, Y.L.; Yu, M. Analysis of insidious fault activation and water inrush from the mining floor. *Int. J. Min. Sci.* **2014**, *24*, 477–483. [CrossRef]

8. Kozyrev, A.; Batugin, A.; Zuo, J.; Zhukova, S. The Impact of Surface Water Seepage on Seismicity and Rockbursting in Mines. *Sustainability* **2022**, *14*, 15414. [CrossRef]

9. Alber, M.; Fritschen, R. Lessons learned from mining-induced seismicity in two deep coal mines. In *ISRM International Symposium-EUROCK 2010*; OnePetro: Richardson, TX, USA, 2010.

10. Yu, Q.G.; Zhang, H.X.; Zhang, Y.J.; Deng, W.N.; Zhang, G.Y. Analysis of fault activation mechanism and influencing factors caused by mining. *J. Chin. Coal Soc.* **2019**, *44*, 18–30.

11. Quevedo, R.; Mejia, C.; Roehl, D. Modelling of fault reactivation in applications of mining and petroleum industry. In *ISRM European Rock Mechanics Symposium-EUROCK 2018*; OnePetro: Richardson, TX, USA, 2018.

12. Donnelly, L.J. A review of international cases of fault reactivation during mining subsidence and fluid abstraction. *Q. J. Eng. Geol. Hydrogeol.* **2009**, *42*, 73–94. [CrossRef]

13. Kong, P.; Jiang, L.; Shu, J.; Wang, L. Mining Stress Distribution and Fault-Slip Behavior: A Case Study of Fault-Influenced Longwall Coal Mining. *Energies* **2019**, *12*, 2494. [CrossRef]

14. Ścigała, R.; Szafulera, K. Linear discontinuous deformations created on the surface as an effect of underground mining and local geological conditions-case study. *Bull. Eng. Geol. Environ.* **2020**, *79*, 2059–2068. [CrossRef]

15. Kaźmierczak, U.; Strzałkowski, P. Environmentally Friendly Rock Mining—Case Study of the Limestone Mine "Górażdże", Poland. *Appl. Sci.* **2019**, *9*, 5512. [CrossRef]

16. Jiang, J.Q.; Wu, Q.L.; Qu, H. Characteristic of mining stress evolution and activation of the reverse fault below the hard-thick strata. *J. Chin. Coal Soc.* **2015**, *40*, 267–277.

17. Nguyen, T.S.; Guglielmi, Y.; Graupner, B.; Rutqvist, J. Mathematical modelling of fault reactivation induced by water injection. *Minerals* **2019**, *9*, 282. [CrossRef]

18. Rutqvist, J.; Graupner, B.; Guglielmi, Y.; Kim, T.; Maßmann, J.; Nguyen, T.S.; Birkholzer, J. An international model comparison study of controlled fault activation experiments in argillaceous claystone at the Mont Terri Laboratory. *Int. J. Rock. Mech. Min.* **2020**, *136*, 104505. [CrossRef]

19. Guglielmi, Y.; Nussbaum, C.; Jeanne, P.; Rutqvist, J.; Cappa, F.; Birkholzer, J. Complexity of fault rupture and fluid leakage in shale: Insights from a controlled fault activation experiment. *J. Geophys. Res. Solid Earth* **2020**, *125*, e2019JB017781. [CrossRef]

20. Jiang, Y.D.; Wang, T.; Zhao, Y.X.; Wang, C. Numerical simulation of fault activation pattern induced by coal extraction. *J. Chin. Univ. Min.* **2013**, *42*, 1–5.

21. Zhao, S.K. Experiments on the characteristics of thrust fault activation influenced by mining operation. *J. Min. Saf. Eng.* **2016**, *33*, 354–361.

22. Ohno, H.; Ishii, E. Effect of fault activation on the hydraulic connectivity of faults in mudstone. *Geomech. Energy Environ.* **2022**, *31*, 100317. [CrossRef]

23. Chen, B.P.; Gong, B.; Wang, S.Y.; Tang, C.A. Research on zonal disintegration characteristics and failure mechanisms of deep tunnel in jointed rock mass with strength reduction method. *Mathematics* **2022**, *10*, 922. [CrossRef]

24. Gong, B.; Wang, Y.Y.; Zhao, T.; Tang, C.A.; Yang, X.Y.; Chen, T.T. AE energy evolution during CJB fracture affected by rock heterogeneity and column irregularity under lateral pressure. *Geomat. Nat. Hazards Risk* **2022**, *13*, 877–907. [CrossRef]

25. Wang, Y.Y.; Gong, B.; Zhang, Y.J.; Yang, X.Y.; Tang, C.A. Progressive fracture behavior and acoustic emission release of cjbs affected by joint distance ratio. *Mathematics* **2022**, *10*, 4149. [CrossRef]

26. Mngadi, S.B.; Tsutsumi, A.; Onoe, Y.; Manzi, M.S.D.; Durrheim, R.J.; Yabe, Y.; Nakatani, M. The effect of a gouge layer on rupture propagation along brittle shear fractures in deep and high-stress mines. *Int. J. Rock Mech. Min.* **2021**, *137*, 104454. [CrossRef]

27. Nguyen, P.T.; Harris, L.B.; Powell, C.M.; Cox, S.F. Fault-valve behaviour in optimally oriented shear zones: An example at the Revenge gold mine, Kambalda, Western Australia. *J. Struct. Geol.* **1998**, *20*, 1625–1640. [CrossRef]

28. Li, Q.F.; Wang, W.J.; Peng, W.Q.; Peng, G. Influence of activation fault after coal extraction on coalmine karst water-inrush. *Chin. J. Rock Mech.* **2010**, *29*, 3417–3424.

29. Delogkos, E.; Roche, V.; Walsh, J.J. Bed-parallel slip associated with normal fault systems. *Earth-Sci. Rev.* **2022**, *230*, 104044. [CrossRef]

30. Hecker, S.; DeLong, S.B.; Schwartz, D.P. Rapid strain release on the Bear River fault zone, Utah–Wyoming—The impact of preexisting structure on the rupture behavior of a new normal fault. *Tectonophysics* **2021**, *808*, 228819. [CrossRef]

31. Steffen, R.; Steffen, H.; Wu, P.; Eaton, D.W. Stress and fault parameters affecting fault slip magnitude and activation time during a glacial cycle. *Tectonics* **2014**, *33*, 1461–1476. [CrossRef]

32. Rupnik, P.J.; Žebre, M.; Jež, J.; Zajc, M.; Preusser, F.; Monegato, G. Deciphering the deformation mechanism in Quaternary deposits along the Idrija Fault in the formerly glaciated Soča Valley, southeast European Alps. *Eng. Geol.* **2022**, *297*, 106515. [CrossRef]

33. Kruszewski, M.; Montegrossi, G.; Balcewicz, M.; Igbokwe, O.A.; Backers, T.; Saenger, E.H. 3D in situ stress state modelling and fault reactivation risk exemplified in the Ruhr region (Germany). *Geomech. Energy Environ.* **2022**, *32*, 100386. [CrossRef]

34. Hong, S.; Sim, H.; Choi, S.J.; Song, Y. Reactivated Timings of the Yangsan Fault in the Yeonghae area based on the Mineralogical Characteristics of Fault Clays. *Econ. Environ. Geol.* **2020**, *53*, 645–654.

35. Molina, O.M.; Zeidouni, M. Analytical model to detect fault permeability alteration induced by fault reactivation in compartmentalized reservoirs. *Water Resour. Res.* **2018**, *54*, 5841–5855. [CrossRef]

36. Clendenin, C.W.; Diehl, S.F. Structural styles of Paleozoic intracratonic fault reactivation: A case study of the Grays Point fault zone in southeastern Missouri, USA. *Tectonophysics* **1999**, *305*, 235–248. [CrossRef]

37. Guo, Y.H.; Luo, L.; Xu, H.H.; Zhu, C. Analysis of the Regularity and Mechanism of Fault Activation Caused by Deep Continuous Mining of Shizishan Copper Mine, China. *Adv. Mater. Sci. Eng.* **2022**, *2020*, 4027231. [CrossRef]

38. Guo, Y.H.; Luo, L. Monitoring and Analysis of Deformation Evolution Law of Fault Activation Caused by Deep Mining in Shizishan Copper Mine, China. *Appl. Sci.* **2022**, *12*, 6863. [CrossRef]

39. Guo, Y.H.; Hou, K.P. Study on Surface Subsidence Law Induced by Deep Mining of Large Steep Metal Deposit. *Appl. Mech. Mater.* **2013**, *295–298*, 2902–2905.

40. Ghosh, G.K.; Sivakumar, C. Application of underground microseismic monitoring for ground failure and secure longwall coal mining operation: A case study in an Indian mine. *J. Appl. Geophys.* **2018**, *150*, 21–39. [CrossRef]

41. Li, T.; Wang, J.A.; Liu, J. Forced thrust mechanism of fault mutation in deep mining. *Chin. J. Rock Mech.* **2014**, *33*, 3760–3765.

42. Zuo, J.P.; Chen, Z.H.; Wang, H.W.; Liu, X.P.; Wu, Z.P. Experimental investigation on fault activation pattern under deep mining. *J. Chin. Coal Soc.* **2009**, *34*, 305–309.

43. Rafiqul, I.M.; Ryuichi, S. Mining-induced fault reactivation associated with the main conveyor belt roadway and safety of the Barapukuria Coal Mine in Bangladesh: Constraints from BEM simulations. *Int. J. Coal Geol.* **2009**, *79*, 115–130.

44. Sainoki, A.; Mitri, H.S. Effect of slip-weakening distance on selected seismic source parameters of min-ing-induced fault-slip. *Int. J. Rock Mech. Min.* **2015**, *34*, 2161–2178.

45. Wei, C.; Zhang, C.; Canbulat, I. Numerical analysis of fault-slip behaviour in longwall mining using linear slip weakening law. *Tunn. Undergr. Space Technol.* **2020**, *104*, 103541. [CrossRef]

46. Lv, Y.X.; Yuan, C.; Zhu, X.H.; Gan, Q.; Li, H.B. THMD analysis of fluid injection-induced fault reactivation and slip in EGS. *Geothermics* **2022**, *99*, 102303. [CrossRef]

47. Haddad, M.; Eichhubl, P. Poroelastic models for fault reactivation in response to concurrent injection and production in stacked reservoirs. *Geomech. Energy Environ.* **2020**, *24*, 100181. [CrossRef]

48. Islavath, S.R.; Katkuri, S.; Deb, D.; Kumar, H. Negotiating an inclined normal fault in a longwall panel: A case study. *Int. J. Coal Geol.* **2022**, *251*, 103935. [CrossRef]

49. Liu, C.; Li, S.; Cheng, C.; Xue, J. Activation characteristics analysis on concealed fault in the excavating coal roadway based on microseismic monitoring technique. *Int. J. Min. Sci. Technol.* **2017**, *27*, 883–887. [CrossRef]

50. Van Balen, R.T.; Kasse, C.; Wallinga, J.; Woolderink, H.A.G. Middle to Late Pleistocene faulting history of the Heerlerheide fault, Roer Valley Rift System, influenced by glacio-isostasy and mining-induced displacement. *Quat. Sci. Rev.* **2021**, *268*, 107111. [CrossRef]

51. Delogkos, E.; Childs, C.; Manzocchi, T.; Walsh, J.J.; Pavlides, S. The role of bed-parallel slip in the development of complex normal fault zones. *J. Struct. Geol.* **2017**, *97*, 199–211. [CrossRef]

52. Guo, Y.H. Study on the Regularity, Mechanism and Deformation Forecast of Rockmass Movement Induced by Caving Mining Steep Deposit in High Stress Area. Ph.D. Thesis, Kunming University of Science and Technology, Kunming, China, 2015.

53. Galderisi, A.; Galli, P. Coulomb stress transfer between parallel faults. The case of Norcia and Mt Vettore normal faults (Italy, 2016 Mw 6.6 earthquake). *Results Geophys. Sci.* **2020**, *1*, 100003. [CrossRef]

54. Collettini, C.; Tesei, T.; Scuderi, M.M.; Carpenter, B.M.; Viti, C. Beyond Byerlee friction, weak faults and implications for slip behavior. *Earth Planet. Sci. Lett.* **2019**, *519*, 245–263. [CrossRef]